

## **A sensitivity study of human mandibular biting simulations using finite element analysis**

Ekaterina Stansfield<sup>1</sup> Jennifer Parker<sup>2</sup> and Paul O'Higgins<sup>1</sup>

<sup>1</sup>Ekaterina Stansfield (corresponding author)

Department of Archaeology and Hull York Medical School the University of York  
John Hughlings Jackson Building, University of York, Heslington, York YO10 5DD, UK  
ekaterina.stansfield@york.ac.uk

<sup>2</sup>Jennifer Parker

Hull York Medical School  
University of York  
jennifer.parker@doctors.org.uk

<sup>1</sup>Paul O'Higgins

Department of Archaeology and Hull York Medical School, the University of York  
John Hughlings Jackson Building, University of York, Heslington, York YO10 5DD, UK  
paul.ohiggins@hyms.ac.uk

**Key words:** Biomechanics; mandible; form and function; Upper Palaeolithic; Mesolithic; FEA; dietary inference.

## Abstract

The form of human mandible reflects both genetic history and loading. In the context of archaeology, it has been used to retrodict loading history as a means of inferring subsistence strategy and paramasticarory use of the dentition. Rather than relying on form to retrodict function, an alternative is to simulate function and compare performance. Finite element analysis (FEA) offers the prospect of predicting and comparing the performance of mandibles under specific loading scenarios, for instance, simulated biting. However, its application depends on the sensitivity of the approach to variation and error in the initial and boundary conditions such as size and shape of the mandible, material properties of the bone tissue, muscle load vectors and the spatial constraints of the model.

In the present paper we investigate the sensitivity of an FE model of a modern human mandible to simplifications in material properties and variations in boundary conditions. A medical CT scan of a living patient is used to create a range of FE digital models with different combinations of material properties, spatial constraints and muscle vectors. We then use ten individual CT scans of human mandibles to create simplified FE models all constrained and loaded in a standard way. We compare the development of von Mises strains over the surface of the mandibles, the output forces at the bite points and the modes and magnitudes global of deformations.

Our results suggest that potential errors in segmentation, muscle force vectors, and constraints can have an appreciable effect on predictions of performance from FE analysis. Therefore, prediction of absolute strain magnitudes is uncertain. However, the errors are not large compared to the differences we find among the sample of mandibles, and FE analysis performs robustly in predicting relative, if not absolute, strains over the surface of a model. We suggest that a sensible approach in future comparative studies is to identically constrain and load 'solid models', comprising one homogenous material (e.g. with the properties of cortical bone). This limits studies to comparison of the effects of varying mandibular external form but such models reasonably predict relative strains, modes of global deformation and bite forces and so allow comparisons of these limited aspects of performance.

## 1. Introduction

The form of the human mandible potentially provides a means by which archaeologists might retrodict mandibular loading history and so infer subsistence strategy and paramasticatory use of the dentition. For instance von Cramon-Taubadel (2011) in a study of global human mandibular variation found that mandibular form reflects subsistence strategy rather than neutral genetic processes, with hunter-gatherers having consistently longer and narrower mandibles than agriculturalists. This finding is significant in the archaeological context since it suggests that, at a population level, the subsistence strategies of past populations might be inferred from the form of the mandible.

An alternative approach to retrodicting diet is to relate morphological variation of the mandible directly to aspects of mechanical performance, assessing how differences in performance relate to differences in masticatory and paramasticatory activity. The classic study of Spencer & Demes (1993) illustrates how basic lever mechanics can be used to assess how differences in size and shape between modern Inuit mandibles and those of Neanderthals would have impacted bite forces and so the ability to use the anterior dentition as tools. More recently Marcé-Nogué et al (2017) found a strong association between mandibular biomechanical performance, mandibular form, food hardness and diet categories in the wider context of primates. This study used finite element analysis (FEA) to assess the ability of primate mandibles to resist biting loads. The methodology involved simulating jaw loading in varying bites and comparing the resulting stresses among mandibles according to the mechanical properties of habitual foods.

Finite element analysis is an engineering technique that calculates stresses and strains produced in an object due to loads applied to it, given the morphology and biomechanical properties of the material (or materials) of the tested body part (Richmond et al., 2005). It potentially provides means to predict and compare the biomechanical performance of skeletal tissues. This is useful in studies of living animals where in vivo experiments may not be possible and in extinct species, whose behaviour we cannot observe directly. FEA may offer a novel approach whereby archaeologists can infer past diets directly; by comparing mechanical performance in simulated biting or paramasticatory loading, rather than form (size and shape) of the mandible. However before a formal assessment of the efficacy of FEA in inferring loading history can be undertaken we need to establish the validity of FEA analyses applied to the mandible and assess the sensitivity of findings to modelling decisions and errors.

FEA simulations of skeletal loading, such as the mandible in biting, are subject to many sources of error that likely impact the resulting predictions of performance. Errors arise in adequately representing the gross anatomy and internal structure as well as variations in material properties, muscle loads and spatial constraints (O'Higgins et al., 2012; Strait et al. 2005; Kober et al., 2004). Thus, Kober et al. (2004) have demonstrated that the anisotropic distribution of bone elasticity (Young's modulus, Poisson's ratio) characteristic of skeletal structures leads to minimisation of stresses and strains that develop in a mandible under masticatory loading conditions. Strait et al. (2005) in a study using a finite-element model of a *Macaca fascicularis* skull found that the model deformed most realistically when orthotropic elastic properties were used but that the extent to which predicted strains matched measured ones was adversely affected when elastic properties

were modelled imprecisely. O'Higgins et al. (2012) noted that variation in the details of bony anatomy, such as the size and orientation of the trabeculae, the thickness of the cortex and the position and orientations of assembled bone fragments has a considerable impact on how virtual models deform under simulated load in FEA. Following this study, Gröning et al. (2012), Fitton et al. (2015) and Toro-Ibacache et al. (2016) showed that alterations in the material properties and simplifications to the internal material structure of the craniofacial models led to marked differences in model performance.

However, Fitton et al (2015) and Toro Ibacache et al (2016) also found that models that greatly simplify internal structure, representing internal anatomy as a solid, homogenous, isotropic material with the properties of cortical bone result in a marked reduction in the magnitudes of predicted strains but have a much smaller impact on the distribution of regions of high and low strain, which indicate mode of deformation. This finding implies that sensible comparative analyses of mode but not magnitude of deformation might be carried out using simplified models. This is important since internal anatomy are rarely knowable due to taphonomic alterations and limitations in CT resolution. Additionally material properties are affected by taphonomic process, so are not known for archaeological and fossil material.

In an ideal situation, a reconstruction of bone internal and external 3D structure that is a close match to the original organism is preferable, while bone mechanical properties (Young's modulus and Poisson's ratio) should be assigned in accordance with their distribution in the living bone of the original organism (Conti et al., 2017; Erdemire et al., 2012). However, for the purposes of biological or evolutionary studies, this approach is not feasible due to the limitations of imaging of anatomical detail and of estimation of material properties throughout a skeletal element. Further, the complexity and scope of the model creation precludes FEA of samples of adequate size to carry out assessments of variation within and among populations. In consequence, most workers employ some degree of simplification of models and or sampling (Ledogar et al., 2017; Ledogar et al. 2016; Godhino et al. 2017, Davis et al. 2011; Toro-Ibacache et al, 2015, Fitton et al. 2015, Smith et al. 2015b).

Considerable intra and inter-individual variation exists in the elasticity of the cortical bone of some regions of the cranial skeleton (Peterson and Dechow, 2003) and mandible (Schwartz-Dabney and Dechow, 2003) as well as in the trabeculae of cancellous bone and in the shapes and sizes of paranasal sinuses (O'Higgins et al., 2012). Nevertheless, it is widely accepted that the level of simplification should be suitable to the question asked of the data (Richmond et al., 2005; Strait et al., 2005, O'Higgins et al., 2012). For instance, biomechanical simulations studying the influence of variations in external morphology can be designed so that internal anatomy, material properties, muscle loads, and constraints are held constant; thus focussing the study on the effects of variations in external form. Nevertheless, it is important to understand the sensitivity of model performance to differences in internal anatomy, material properties and boundary conditions before simplifying these parameters.

Prior studies (Godhino et al., 2017; Toro-Ibacache et al., 2016; Evans et al., 2012; Parr et al., 2012; Wood et al., 2011; Wroe et al., 2010; Wroe et al., 2007; Rayfield, 2007) considered the validity and sensitivity of FEA to varying input parameters in finite element models of the cranium. They have shown that FEA results are very sensitive to variations in input parameters and so, great care is

required when comparing results among different models. Gröning et al. (2011a) and Gröning et al. (2012) undertook an assessment of the validity and sensitivity of a single mandibular finite element model to variations in how cancellous bone and the periodontal ligament are represented, as well as to constraints and the orientation of applied muscle forces. Equally, Toro-Ibacache et al. (2015) have shown that variation in the modelling of trabecular structure such as might occur due to limitations in 3D imaging and error have a significant impact on absolute values of stresses and strains, though less on relative magnitudes among cranial regions. These authors concluded that most effects are potentially large enough to render FEA prediction of absolute, but not relative strain magnitudes problematic. Nevertheless, Gröning et al. (2011b) used FEA to assess the biomechanical significance of the human chin using an FEA in a study that was carefully designed to control for unknown parameters.

These considerations of error aside, there is evidence that FEA is a useful tool in reproducing mandibular loading resistance and so aspects of diet (Bourke et al., 2008; Moreno et al., 2008; Cox et al., 2012; Marcé-Nogué et al., 2017; Tsouknidas et al., 2017). However, it also appears that accurate modelling is impossible and predictions from FEA are very sensitive to input parameters. In the present study we explore the sensitivity of mandibular FEA simulations of biting to modelling decisions. Our aim is to establish and understand the limitations and impacts of different modelling choices on the performance of models of the mandible. We do this to assess how best to model and simulate biting and to understand what aspects of performance can reliably be predicted in comparative studies. Such a framework is of obvious importance in the interpretation of the mandibular remains of past populations in relation to diet and paramasticatory activities.

Unlike in engineering, where the performance of individual structures is of interest, biological problems are mostly concerned with comparisons between organisms and with the study of intra and inter-group variation. For example, several recent papers (Ledogar et al. 2017; Smith et al. 2015a; Strait et al. 2013; Gröning et al., 2011b; Wroe et al. 2010; Strait et al. 2009) have compared the biomechanics of mastication among australopithecines, humans and apes. Other authors have compared Neanderthals and modern humans (Zink and Lieberman, 2016; O'Connor et al, 2005; Spencer and Demes, 1993) or have examined variations within modern humans (Ledogar et al. 2016). It is therefore important that sources of error in the biological application of finite element analysis are understood in sufficient detail to be able to distinguish likely error from dietary signal in multi-individual comparisons.

With this in mind, the present paper investigates the sensitivity of an FE model of a modern human mandible to simplifications in material properties and variations in boundary conditions. By permuting material properties and varying boundary conditions we assess the ranges of variation of predicted aspects of performance and compare these with the variations in performance encountered among a sample of modern human mandibles modelled and loaded according to a standardised and simplified protocol.

We test the following four hypotheses:

H1: That variations in material properties and spatial constraints have no impact on performance assessed in terms of deformation and biting forces.

H2: That variations in muscle force vectors have no impact on performance assessed in terms of deformation and biting forces.

H3: That variations in mandibular form (size and shape) have no impact on performance assessed in terms of deformation and biting forces.

We expect each of these to be falsified and are interested to know (i) the impact of these factors on the mode and magnitude of deformation of a mandible under simulated biting and (ii) if these impacts are large or small when compared to the differences in performance among a sample of human mandibles. Our aim is to provide a reference against which apparent differences in predicted performance among modern and ancient human mandibles can be assessed.

## 2. Material and Methods

### 2.1. Material

Nine dry mandibular CT scans (labelled here as DM1-9) were sourced from the anatomical collection of the Hull York Medical School: 7 medical CT scans of dry teaching mandibles scanned at York District Hospital (slices/voxel size: 306/0.24 x 0.24 x 0.4), one medical CT scan of a dry mandible obtained at a higher resolution (817/ 0.15 x 0.15 x 0.15), and 1 dry mandible micro CT scan in which the specimen had been scanned in two halves (889/ 0.12 x 0.12 x 0.12). A further CT scan of a living male, who gave his consent to scientific investigations, was obtained with clearance from the ethics committee of Moscow State University. The resolution of this scan was 0.468, 0.468, 0.3 mm. The quality of the CT scan allowed estimation of the muscle force vectors. The mandible segmented from this scan is the 'test mandible' used to assess sensitivity to segmentation, spatial constraints and loadcase.

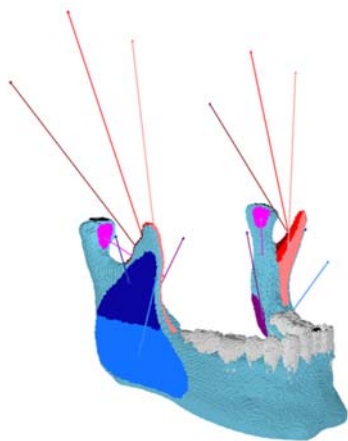
All CT scans were segmented as described below and used to build 3D surface and voxel based reconstructions. The shapes and sizes of the mandibular surface models were quantified using 35 fixed landmarks (Table 1) using the EVAN Toolbox (<http://www.evan-society.org>). The voxel based reconstructions were then re-sampled to cubic voxels of size 0.5mm x 0.5mm x 0.5mm to ensure comparability among models and because the FEA software, VoxFE (the latest version of which is available at <https://sourceforge.net/projects/vox-fe/>), requires cubic voxels for mesh conversion. All mandibles were oriented so that their occlusal planes coincided in the x, y plane. Once imported into VoxFE different material properties and loadcases (Figure 1), as described below, were applied, simulating right first incisor or second molar biting using the muscle forces listed in Table 2 for most analyses.

Table 1. Landmarks

No	Name	No	Name
1	Gnathion	20	Coronion left
2	Infradentale	21	Coronion right
3	Linguale	22	Sigmoid notch left
4	Orale Mandibular	23	Sigmoid notch right
5	Pogonion	24	Gonion left
6	Mental foramen anterior left	25	Gonion right

7	Mental foramen anterior right	26	Ramus posterior in line with alveolus left
8	C-P3 left	27	Ramus posterior in line with alveolus right
9	C-P3 right	28	Mandibular foramen inferior right
10	P4-M1 left	29	Mandibular foramen inferior left
11	P4-M1 right	30	Condyle central condyle left
12	M1-M2 left	31	Condyle central condyle right
13	M1-M2 right	32	Condyle lateral left
14	Alveolar process distal buccal left	33	Condyle lateral right
15	Alveolar process distal buccal right	34	Condyle medial left
16	Alveolar process distal lingual left	35	Condyle medial right
17	Alveolar process distal lingual right		
18	Ramus root left		
19	Ramus root right		

**Figure 1.** An FEA project in VoxFE: coloured patches show muscle attachments, lines indicate muscle vectors. The right first molar is constrained in the vertical direction, while condyles are constrained in all directions.



## 2.2. Muscle vectors

Four muscles were included in the analysis: masseter, temporalis, medial pterygoid and inferior lateral pterygoid. These last two are represented in the FE model as single vectors passing from origin to insertion. Masseter was represented as separate vectors for superficial and deep portions, the former arising from the lower part of the external surface of the ramus, the latter from the upper surface with both directed towards the zygomatic arch; the superficial masseter vector anteriorly and the deep posteriorly. Temporalis was also represented by a series of vectors representing anterior, middle and posterior portions, taking origin from anterior, middle or posterior portions of the temporal muscle attachment area on the cranium and inserting in the same order on the coronoid (see Figure 1). With the right side taken as the working side, the force activation patterns corresponded to single-tooth bites as detailed by Nelson (1986), while the maximum muscle force was estimated by Groening et al. (2011b) on the basis of the muscle physiological cross-sectional

areas (PCSA) of the masticatory muscles (van Eijden et al., 1995, 1996). Table 2, therefore, lists each muscle vector maximum force and activation used in this study.

Table 2. Maximal muscle forces and the scaling factors applied to simulate different bites\*\*

	Maximum	First incisor		First molar	
	force	left	right	left	right
<b>Superficial masseter</b>	218	0.4	0.4	0.6	0.72
<b>Deep Masseter</b>	112	0.26	0.26	0.6	0.72
<b>Anterior temporalis</b>	168	0.08	0.08	0.58	0.73
<b>Middle temporalis</b>	137	0.06	0.06	0.67	0.66
<b>Posterior temporalis</b>	119	0.04	0.04	0.39	0.59
<b>Medial pterygoid</b>	192	0.78	0.78	0.6	0.84
<b>Inferior lateral pterygoid</b>	90	0.71	0.71	0.65	0.3

\*\*Groening et al (2011b).

Muscle force vectors were estimated from the coordinates of the centroids of muscle insertions on the mandible and cranium, directly estimated from the CT scan of the living human, and using a Microscribe 3DX for the nine skulls from the anatomical collection. To ensure a fair test (i.e. to control for everything except mandibular form), the same average muscle vectors were then applied to each mandible in all the sensitivity analyses, except those that assessed sensitivity to muscle vectors, the details of which are given below.

To calculate the average muscle vectors, in each dry specimen and in the CT scan of the living individual, landmarks of the centres of muscle origin and insertion were digitised along with a number of anatomical landmarks on the combined mandible and cranium with the jaw closed. The data were then superimposed (translated and rotated) using three landmarks: Alveolar process distal buccal left, Alveolar process distal buccal right and Infradentale. The average vectors between muscle insertion and origin were then calculated across all 10 individuals. In each model these average vectors were then translated such that they took origin at each estimated muscle centroid (Figure 1).

### 2.3. Models and loadcases

The different models and loadcases are detailed in Table 3 and discussed below in relation to each hypothesis.

Table 3. FE tests of sensitivity and their conditions.

Test	Material	Independent variable	Fixed variables
------	----------	----------------------	-----------------



<b>Test of sensitivity to different material properties</b>	CT scan of the test mandible	Material properties of cortical bone, teeth, periodontal ligament ("PDL") and cancellous bone are varied.	The form of the mandible (size and shape), muscle vectors, muscle activation pattern, spatial constraints at the condyles and the biting tooth.
<b>Test of sensitivity to muscle vector orientations</b>	CT scan of the test mandible	Muscle vectors are varied within 2 standard deviations from the average for different muscles.	The form of the mandible (size and shape), material properties, muscle activation pattern, spatial constraints at the condyles and the biting tooth.
<b>Test of sensitivity to spatial constraints applied to condyles and the biting tooth.</b>	CT scan of the test mandible	Spatial constraints of the condyles and the biting tooth.	The form of the mandible (size and shape), material properties, muscle vectors, muscle activation pattern.
<b>Test of sensitivity to the form of the mandible</b>	CT scans of the nine dry mandibles and the CT scan of the test mandible	Individuals	The form of the mandible (size and shape), material properties, muscle vectors, muscle activation pattern, spatial constraints at the condyles and the biting tooth.

### 2.3.1. Test of sensitivity to different material properties

The CT scan of the living male (the 'Test Mandible') was segmented in detail, using Avizo ©, to distinguish four 'materials' : cortical bone, cancellous bone, periodontal ligament and the teeth (Table 3). Cortical bone and teeth were segmented semi-automatically by establishing initial segmentation thresholds and then refining these by hand. The segmentation of cancellous bone and periodontal ligament involved informed decisions (because of CT quality/resolution) on the probable extent of the tissue. Thus, cancellous bone was segmented as a bulk material, regardless of its internal structure and periodontal ligament, which is thinner than the resolution of our models, was simulated as a 1-2 voxel layer between tooth dentine and the surrounding cancellous or cortical bone (Gröning et al., 2011b).

To assess the sensitivity of the FE model to varying segmentations we allocated different material properties as shown in Table 4, to different materials as listed in Table 5. In effect we compared models with varying numbers of materials ranging from 3 (cortical bone, teeth, cancellous bone/PDL) to 1 (cortical bone). The model was constrained at the condyles by fixing 60 nodes on the centre of each of the condyles in x, y and z directions and by 40 ( $I_1$ ) or 50 ( $M_2$ ) nodes on the loaded tooth fixed in the vertical (y) direction only. The finite element models were then solved and the results were obtained as landmark coordinates on the deformed mandible, von Mises strains and strain maps.

Table 4. Material properties assigned to different structures.

<i>Material</i>	<i>Young's modulus</i>	<i>Poisson Ratio</i>	<i>References</i>
<b>Cortical bone</b>	17 GPa	0.3	Meredith, et al. 1996; Peterson &
<b>Teeth</b>	50 GPa	0.3	Dechow, 2003; Horgan & Gilchrist, 2003;
<b>Cancellous bone</b>	0.5 GPA*	0.3*	Wang et al., 2006; Wroe et al. 2010;
<b>PDL</b>	0.5 GPA*	0.3*	Groning et al., 2009, 2011;
<b>TMJ soft tissue</b>	0.5 GPA*	0.3*	Barak, et al. 2009; Benazzi et al. 2012; Jansen van Rensburg et al. 2012.

\* The literature offers a wide range of values of Young's modulus for cancellous bone, PDL and TMJ soft tissue, with Young's Modulus ranging 0.1-100 MPa and Poisson's ratio up to 0.49 (Groening et al., 2011; Beek et al. 2000, Chen et al. 1998, Koolstra and van Eijden 2005, Tanne et al. 1991; Andersen et al. 1991, Cattaneo et al. 2005 ; Dorow et al. 2003 ; Jones et al. 2001, Poppe et al. 2002, Tanne et al.1987).

Table 5. Combinations of material properties and constraints for different cases. See text for further details.

<i>Abbreviation</i>	<i>Material properties and constraints</i>
<b>TCCP</b>	<b>Teeth, Cortical bone, Cancellous bone plus PDL</b> (Cancellous bone and PDL are allocated the same material properties), standard constraints.
<b>TCC</b>	<b>Teeth, Cortical bone, Cancellous bone</b> (PDL is combined with and allocated the same material properties as cortical bone), standard constraints.
<b>TCP</b>	<b>Teeth, Cortical bone, PDL</b> (cancellous bone is allocated the same material properties as cortical bone), standard constraints.
<b>TC</b>	<b>Teeth, Cortical bone</b> (cancellous bone and PDL are allocated the same material properties as cortical bone), standard constraints.
<b>C</b>	<b>Cortical bone</b> , (teeth, cancellous bone and PDL are allocated the same material properties as cortical bone), standard constraints.
<b>TCCP SC</b>	<b>Teeth, Cortical bone, Cancellous bone plus PDL, small number of nodes</b> (10) constrained at the <b>condyles</b> , standard constraints on the teeth.
<b>TCCP ST</b>	<b>Teeth, Cortical bone, Cancellous bone plus PDL, small number of nodes</b> (10) constrained at the <b>teeth</b> , standard constraints on the condyles.
<b>TCCP TMJ</b>	<b>Teeth, Cortical bone, Cancellous bone plus PDL, condyles</b> are constrained within a segmented <b>temporo-mandibular joint</b> , standard constraints at teeth.
<b>TCCP box</b>	<b>Teeth, Cortical bone, Cancellous bone plus PDL, condyles</b> are constrained by an artificial <b>box</b> , standard constraints at teeth.

### 2.3.2. Test of sensitivity to spatial constraints applied to condyles and the biting tooth

We applied spatial constraints to the Test Mandible to simulate the point in the masticatory cycle when the right first incisor or second molar tooth is in contact with a small and hard food object and with very small gape. At small gapes the mandibular condyles lie in the depth of the temporo-mandibular joint (TMJ) (Klooststra, Van Eijen, 1997). This is simulated by fixing the position of the mandibular joint in x, y, and z directions (in different ways, see below), while constraining the

movement of the loaded tooth in the vertical (z) direction. 40 nodes were constrained on I<sub>1</sub> to simulate incisor biting and 50 nodes on M<sub>2</sub> to simulate molar biting.

The test mandible FE model was constrained at the condyles in different ways: (a) by including in the model part of the temporal bone above the TMJ and the soft tissue layer between the condyle and the joint surface. The material properties of cortical bone are allocated to the temporal bone part and the soft tissue in the TMJ was allocated the material properties of periodontal ligament (Table 4) which is within the range of published values for the soft tissue of the TMJ (Tanne et al., 1991; Chen et al., 1998; Beek et al., 2000; Koolstra and van Eijden, 2005) (see Table 3); (b) by creating an artificial block of material with the properties of cortical bone and attaching it to the mandibular condyles via a 3 mm thick layer of soft tissue with the material properties of periodontal ligament (following Gröning et al. 2011a); (c) by directly constraining 60 nodes on the antero-central portion of the surface of the right and the left condyles (d) by directly constraining only 10 nodes in the same position. In (a) and (b) the position of the material above the 'TMJ' was fixed in all three axes by fixing several nodes at the four corners of the 'bony' part. In cases (c) and (d) the nodes on the condylar surfaces were fixed along the three axes.

To assess the effects of varying constraints on the teeth, the model with mandibular condyles constrained at 60 nodes on the antero-central portion of the condylar surfaces was modified by reducing the number of nodes that constrained the loaded tooth (originally 40 nodes on I<sub>1</sub> and 50 nodes on M<sub>2</sub>) to 10.

#### Test of sensitivity to muscle vector orientations

The sensitivity of the test mandible to variations in muscle vectors was assessed in simulated incisor bites for simultaneous shifts of muscles vectors in all three axes and for shifts of each masticatory muscle, one at a time. For molar biting only the effects of shifting all muscles simultaneously are assessed. After translation of the attachment to the mandible of each muscle vector, as described above the coordinates of muscle attachment *on the cranium* were varied by + or – 2 standard deviations of x, y or z coordinates from the average landmark location (Table 6).

Table 6. The load cases used in the sensitivity analyses. The vectors of muscle action are modified by varying the coordinates of muscle attachments *on the cranium* by +2 or – 2 standard deviations from their mean as estimated using the 10 individuals in the study

Name	Description
<b>I1 standard</b>	Incisor bite, all muscles in standard orientation
<b>I1 all ant</b>	Incisor bite, for all muscles the lower 'y' coordinate used
<b>I1 all post</b>	Incisor bite, for all muscles the higher 'y' coordinate used
<b>I1 all inf</b>	Incisor bite, for all muscles the lower 'z' coordinate used
<b>I1 all sup</b>	Incisor bite, for all muscles the higher 'z' coordinate used
<b>I1 all med</b>	Incisor bite, for the left muscles the lower 'x' coordinate used, for the right muscles, the higher 'x' coordinates used
<b>I1 all lat</b>	Incisor bite, for the left muscles the higher 'x' coordinate used, for the right muscles, the lower 'x' coordinate used.
<b>I1 lat pter ant</b>	Incisor bite, all muscles in standard orientation except the lateral pterygoids where the lower 'y' coordinates are used
<b>I1 lat pter post</b>	Incisor bite, all muscles in standard orientation except the lateral pterygoids

---

	where the higher 'y' coordinates are used
<b>I1 lat pter inf</b>	Incisor bite, all muscles in standard orientation except the lateral pterygoids where the lower 'z' coordinates are used
<b>I1 lat pter sup</b>	Incisor bite, all muscles in standard orientation except the lateral pterygoids where the higher 'z' coordinates are used
<b>I1 lat pter med</b>	Incisor bite, all muscles in standard orientation except the lateral pterygoids where the left muscles use the lower 'x' coordinate, and the right muscles use the higher 'x' coordinate
<b>I1 lat pter lat</b>	Incisor bite, all muscles in standard orientation except the lateral pterygoids where the left muscles use the higher 'x' coordinate, and the right muscles use the lower 'x' coordinate
<b>I1 m pter ant</b>	Incisor bite, all muscles in standard orientation except the medial pterygoids where the lower 'y' coordinate is used
<b>I1 m pter post</b>	Incisor bite, all muscles in standard orientation except the medial pterygoids where the higher 'y' coordinate is used
<b>I1 m pter inf</b>	Incisor bite, all muscles in standard orientation except the medial pterygoids where the lower 'z' coordinate is used
<b>I1 m pter sup</b>	Incisor bite, all muscles in standard orientation except the medial pterygoids where the higher 'z' coordinate is used
<b>I1 m pter med</b>	Incisor bite, all muscles in standard orientation except the medial pterygoids where the left muscles use the lower 'x' coordinate, and the right muscles use the higher 'x' coordinate
<b>I1 m pter lat</b>	Incisor bite, all muscles in standard orientation except the medial pterygoids where the left muscles use the higher 'x' coordinate, and the right muscles use the lower 'x' coordinate
<b>I1 mass ant</b>	Incisor bite, all muscles in standard orientation except the superficial and deep masseters where the lower 'y' coordinates are used
<b>I1 mass post</b>	Incisor bite, all muscles in standard orientation except the superficial and deep masseters where the higher 'y' coordinates are used
<b>I1 mass inf</b>	Incisor bite, all muscles in standard orientation except the superficial and deep masseters where the lower 'z' coordinates are used
<b>I1 mass sup</b>	Incisor bite, all muscles in standard orientation except the superficial and deep masseters where the higher 'z' coordinates are used
<b>I1 mass med</b>	Incisor bite, all muscles in standard orientation except the superficial and deep masseters where the left muscles use the lower 'x' coordinate, and the right muscles use the higher 'x' coordinate
<b>I1 mass lat</b>	Incisor bite, all muscles in standard orientation except the superficial and deep masseters where the left muscles use the higher 'x' coordinate, and the right muscles use the lower 'x' coordinate
<b>I1 temp ant</b>	Incisor bite, all muscles in standard orientation except the anterior, middle and posterior temporalis where the lower 'y' coordinates are used
<b>I1 temp post</b>	Incisor bite, all muscles in standard orientation except the anterior, middle and posterior temporalis where the higher 'y' coordinates are used
<b>I1 temp inf</b>	Incisor bite, all muscles in standard orientation except the anterior, middle and posterior temporalis where the lower 'z' coordinates are used
<b>I1 temp sup</b>	Incisor bite, all muscles in standard orientation except the anterior, middle and posterior temporalis where the higher 'z' coordinates are used
<b>I1 temp med</b>	Incisor bite, all muscles in standard orientation except the anterior, middle and posterior temporalis where the left muscles use the lower 'x' coordinate, and the right muscles use the higher 'x' coordinate
<b>I1 temp lat</b>	Incisor bite, all muscles in standard orientation except the anterior, middle and

---

	posterior temporalis where the left muscles use the higher 'x' coordinate, and the right muscles use the lower 'x' coordinate
<b>M2 standard</b>	Second molar bite, all muscles in standard orientation
<b>M2 all ant</b>	Second molar bite, for all muscles the lower 'y' coordinates are used
<b>M2 all post</b>	Second molar bite, for all muscles the higher 'y' coordinates are used
<b>M2 all inf</b>	Second molar bite, for all muscles the lower 'z' coordinates are used
<b>M2 all sup</b>	Second molar bite, for all muscles the higher 'z' coordinates are used
<b>M2 all med</b>	Second molar bite, for the left muscles the lower 'x' coordinates are used, for the right muscles the higher 'x' coordinates are used
<b>M2 all lat</b>	Second molar bite, for the left muscles the higher 'x' coordinates are used, for the right muscles the lower 'x' coordinates are used

The resulting finite element models from the sensitivity analyses described above were solved using Vox-FE. Strains at nodes, strain maps landmark coordinates on the deformed mandibles were recorded for subsequent analyses

### 2.3.3. Test of sensitivity to the form of the mandible

The foregoing tests examine the effects on a single mandible of varying material properties, muscle vectors and constraints. The variations produced as a result of these differences need to be set against the range of variation we might expect in a sample of mandibles, to know if error is relatively large or small. To achieve this, the CT scans of the nine dry mandibles were each segmented as a single solid material and allocated the material properties of cortical bone, as for C5 in Table 4. All models were loaded with identical muscle forces in each bite (Table 2) and with the mean muscle vectors while spatial constraints comprised the standard 40 nodes on  $I_1$  and 50 nodes on  $M_2$  constrained in the vertical, z direction and the condyles constrained by fixing 60 nodes on the central portion of the surface of the right and the left condyle as in our standard case of constraints.

## 2.4. Analyses

The results of the FEAs comprised von Mises strains, forces at constraints, and the coordinates of the 35 landmarks (Table 1) on each undeformed and deformed model. These results were used to:

- (1) Draw contour maps of von Mises strains to allow a visual comparison among models.
- (2) Compare biting forces among model variants.
- (3) Plot von Mises strains at anatomical landmark points (Table 1).
- (4) Carry out analyses of size and shape differences between unloaded and loaded models (= deformation) using the coordinates of these landmarks (Table 1) in the unloaded and loaded models. We followed the protocol developed in previous papers (O'Higgins et al., 2011, 2012; Milne and O'Higgins, 2012; O'Higgins and Milne, 2013). The coordinates of all unloaded and loaded mandibles were first subjected to generalised Procrustes analysis (GPA) and then rescaled to their original centroid sizes to obtain size and shape variables. Next, the differences in landmark coordinates between the loaded and unloaded models were calculated by subtraction. To facilitate the visualisation of results, these were then added to the average unloaded form obtained by averaging the shape variables and multiplying these by the average centroid size. Finally, to visualise the modes and magnitudes of deformation, a principal component analysis (PCA) was carried out of the

mean unloaded mandibular size and shape together with the new representations of the loaded mandibles referred to this mean. The choice of unloaded model for visualisation does not impact the (Procrustes size and shape) distances computed among models (or the scatters in the PC plots). This space exactly represents deformations but variances scale with size. However, over the small deformations arising in FEA, the nonlinearity is not of great importance.

- (5) Assess the magnitude of 'errors' in modelling due to differences in segmentation and loadcase by computing the variance in Procrustes size and shape distances. This is compared with the variance arising from differences in form by expressing it as a percentage.
- (6) Assess how deformation of the mandible in each biting simulation is associated with mandibular form. First, a crude estimate is obtained by computing the correlations between the matrix of Procrustes size and shape distances among mandibles (mandibular shape variables from GPA, rescaled by centroid size) and the matrices of differences in deformation among mandibles (Procrustes size and shape distances among deformations referred to the mean form calculated in 4, above. Second, a detailed analysis was carried out using 2-block partial least squares (PLS) analysis in which one block is the size and shape variables of the unloaded mandibles and the other is the size and shape variables of the loaded mandibles referred to the mean. These size and shape variables are those calculated in 4, above. This allowed us to assess both the degree and the nature of any such association (i.e what aspects of form are associated with what modes of deformation) and to visualise these associations as warpings of the mean form and mean deformation-

### 3. Results

#### 3.1. Biting forces

Tables 7, 8 and 9 present values of incisor and molar bite forces arising in each FEA simulation of biting in the test mandible and among individuals. In general the differently segmented, loaded and constrained models of one individual show variation in biting force magnitude ranging between 170N and 194N for central incisor bites and 633N and 691N for molar. As assessed for incisor bites (Table 8), shifting all muscle vectors simultaneously has a greater effect than shifting just one. The ranges of variation of bite forces are, however, small with respect to their magnitudes (mean for central incisor bites = 181N, mean for second molar bites = 662N) and with respect to the variation in predicted biting forces among individuals (Table 9), where force magnitudes range from 146N to 214N for the central right incisor and from 508N to 705N for the second right molar.

Table 7. Bite forces (N) produced in the Test Mandible in the study of sensitivity to materials and constraints. Column headings refer to combinations of material properties and constraints for different cases as listed in Table 5

	TCCP	TCCP SC	TCCP ST	TCCP TMJ	TCCP box	TCC	TCP	TC	C	Average	Variance	% of variance among individuals (Table 9)
<b>I1</b>	182	187	181	170	194	181	174	182	181	181	41.8	10.6
<b>M2</b>	698	698	704	633	713	698	681	698	696	691	482	7.8

Table 8. Bite forces produced in the study of sensitivity to muscle vector directions.

Bite forces (N) with mean vectors	Muscles changed	Bite forces (N) when muscle vectors are shifted in varying directions *						Mean Bite Force	Variance	% of variance among individuals (Table 9)
		<i>Anteriorly</i>	<i>Posteriorly</i>	<i>Superiorly</i>	<i>Inferiorly</i>	<i>Medially</i>	<i>Laterally</i>			
		Bite Force on Right I <sub>1</sub> (N)								
150.01	All	183.6	113.8	148.0	152.1	150.8	148.9	149.6	349.3	88.4
	Masseter	161.8	136.2	147.8	152.4	151.4	148.4	149.7	49.3	12.5
	Lateral Pterygoid	151.0	148.8	150.4	149.6	149.7	150.3	150.0	0.42	0.11
	Temporalis	151.6	148.5	150.4	149.6	155.0	150.0	150.7	3.78	0.96
	Medial Pterygoid	169.3	130.4	149.5	150.6	149.6	150.4	150.0	108.0	27.3
		Bite Force on Right M <sub>2</sub> (N)								
597.888	All	702.3	485.6	597.7	597.7	602.9	591.7	596.6	3365.2	54.6

\* Vectors are shifted along each of the three axes by two standard deviations of the according landmark coordinate (see Methods chapter for details). Here, medio-lateral direction is described by the x-axis, antero-posterior direction is the y-axis and superior-inferior direction is described by the z-axis.



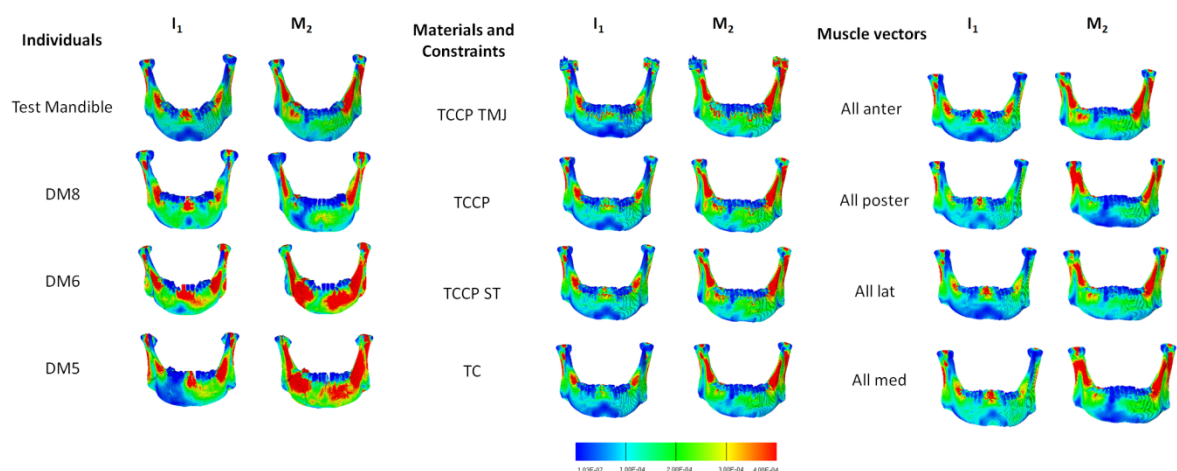
Table 9. Bite forces (N) produced in the study of sensitivity to individual differences.

	DM1	DM2	DM3	DM4	DM5	DM6	DM7	DM8	DM9	Test Mandible	Average	Variance
I1	157	161	150	152	185	181	214	170	146	181	170	395.2
M2	589	525	508	630	649	719	757	643	558	696	627	6164.2

### 3.2. Strain analysis

Example strain maps from the sensitivity analysis of variations in material properties are presented in Figure 2. These indicate that segmentation and allocation of material properties have an effect on strain magnitudes and on the mode of deformation, the distribution of regions of low and high strain. Similarly, variations in muscle force vectors and in spatial constraints have an effect on magnitudes of von Mises strain and on the mode of deformation (the strain contour maps) as also shown in Figure 2.

**Figure 2.** Examples of von Mises strain maps for studies of the impact on biting performance of variations in material segmentation, constraints and muscle vectors in one individual.



In all the sensitivity analyses (rightmost and central columns of Figure 2), the mandible experiences localised peak strains, similar in size among incisor and among molar loadings between the alveolar process and the root of the mandibular ramus and in the area below the loaded tooth. The presence of a PDL reduces the peaks of strain so that smaller areas of the body and the ramus experience high strains. Of critical importance in the context of this study is the extent to which the predictions of strains from FEA are affected by the modelling decisions that underlie the sensitivity analyses: are the effects large or small when compared to the differences among different mandibles modelled and loaded in identical ways? Comparing the strain contour maps from the sensitivity analyses in a single individual (rightmost and central columns of Figure 2) with those for different individuals (leftmost column of Figure 2) the magnitudes and distributions of regions of high and low strain show marked differences between individuals relative to those encountered in the sensitivity study.

The magnitudes of von Mises strains at 27 landmarks are presented in the appendix (Figures A.1, A.2 and A.3), strains at the six landmarks (#28-33; Table1) on the condyles are omitted because they are

very close to, or at, constraints, resulting in large, highly localised, variations. Table 10 presents the variances in these 27 von Mises strains that arise in the studies of sensitivity and variations within our sample. In the sensitivity analyses of constraints and material property combinations (segmentations), variances in the von Mises strains are mostly somewhat less than 10% of the variance among different individuals (Table 10). The largest variance (18% of the variance among individuals) in the sensitivity analyses arises when the spatial constraints are modified while biting on the second molar.

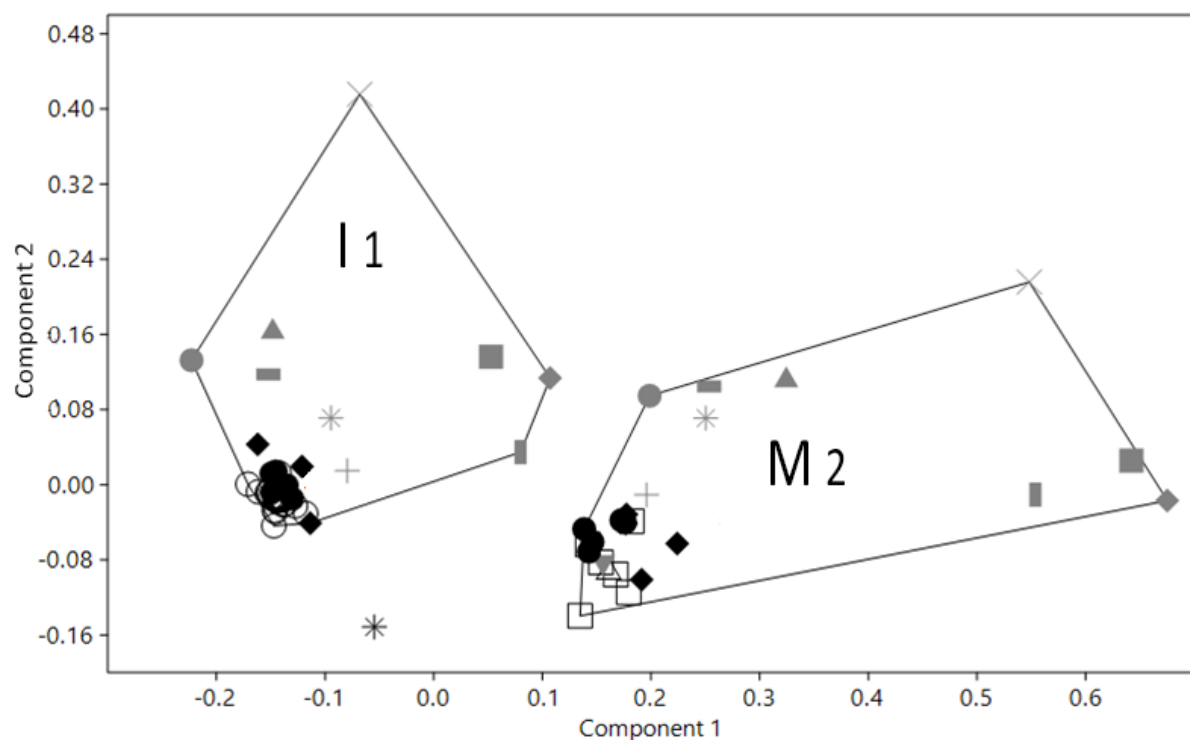
Table 10. Variance in von Mises strains at 29 landmarks (6 landmarks at the condyles are excluded).

Study	I1		M2	
	<i>Average Variance in von Mises Strains</i>	<i>% of the variance between individuals</i>	<i>Average Variance in von Mises Strains</i>	<i>% of the variance between individuals</i>
Different individuals	$5.6 \times 10^{-8}$	100	$3.28 \times 10^{-8}$	100
Segmentation in one individual	$0.11 \times 10^{-8}$	1.9	$0.24 \times 10^{-8}$	7.5
Constraints in one individual	$0.20 \times 10^{-8}$	3.6	$0.60 \times 10^{-8}$	18
Muscle vectors in one individual	$0.035 \times 10^{-8}$	6.2	$0.27 \times 10^{-8}$	8.3

### 3.3. Global deformations; changes in size and shape with loading

Modes and magnitudes of deformation are compared through PCA of size and shape variables from the mean unloaded mandible and the loaded mandibles referred to the mean. The first two principal components are plotted in Figure 3. The first PC explains 69%, the second, 12%, the third, 8% and fourth, 4% of the total variance. The first two components (80.7% of the total variance) show that the differences among different versions of the test mandible, segmented, loaded and constrained in different ways are small relative to the variations in deformation encountered among the sample of individuals, with the variants of the test mandible occupying approximately 10-15% of the area in the plot occupied by different individuals.

**Figure 3.** PCA of size and shape: Combined sensitivity study. Deformations of a single specimen segmented in different ways and subjected to different muscle vectors plotted with data from different individuals loaded to simulate 1<sup>st</sup> incisor and 2<sup>nd</sup> molar biting using specific activation patterns for each bite. PC1/PC2 (81.4% of variation). Black circles: sensitivity to segmentation; black rhomboids: sensitivity to constraints of the tooth and the condyles; black circular ( $I_1$ ), and square ( $M_2$ ) outlines: sensitivity to muscle vector directions; solid grey markers: different individuals. Black asterix=unloaded mandible.



In Table 11 the variance in Procrustes size and shape distances among differently modelled and loaded versions of the test mandible is expressed as a percentage of the variance arising from differences in form. This shows that the variance in deformations due to varying constraints and the combination of materials accounts for approximately 5.2% of the variance among individuals for a molar bite and 6.8% for incisor. These errors are of similar magnitude to those arising from variations in muscle vectors for molar bites and ~15x larger than those for incisor bites (0.39%).

Table 11. The variance in Procrustes size and shape distances in the 29 landmarks (landmarks on condyle are excluded) due to differences in segmentation and loadcase expressed as a percentage of the variance in size and shape among the 10 mandibles\*. Here, the studies of segmentations' and constraints' variations are put together.

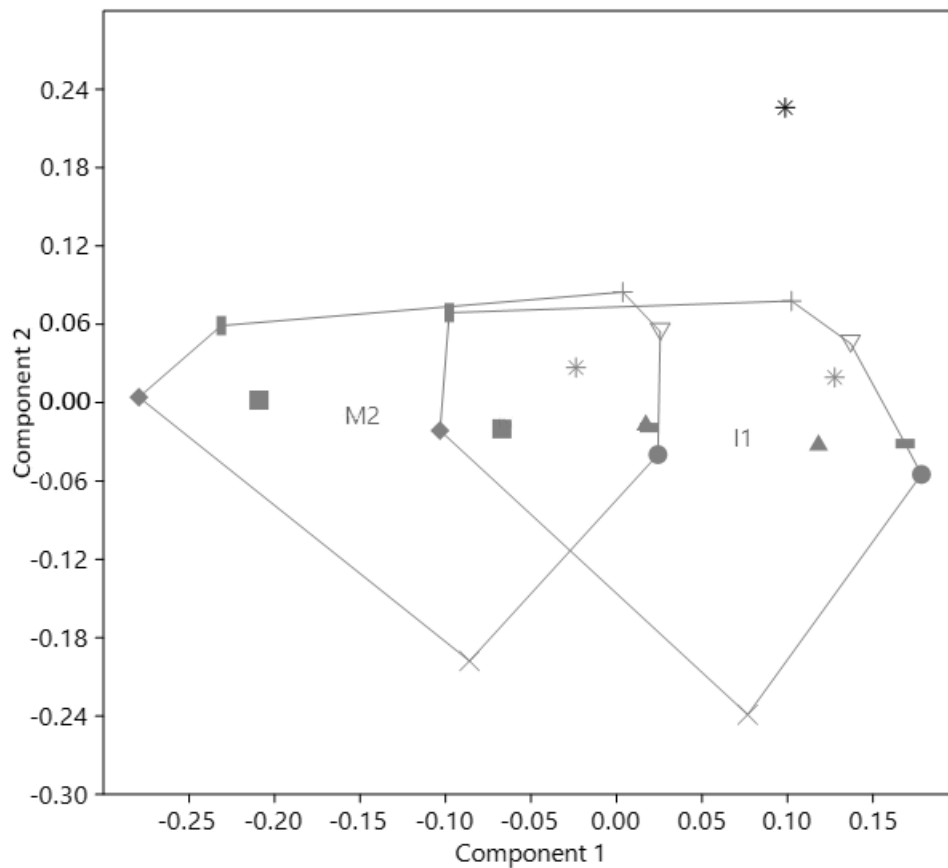
	I1		M2	
	<i>Variance</i>	<i>% Variance due to differences in form</i>	<i>Variance</i>	<i>% Variance due to differences in form</i>
<b>Different individuals</b>	0.003480	100	0.00780	100
<b>Constraints and segmentation in one individual</b>	0.000236	6.78	0.00041	5.21
<b>Muscle vectors in one individual</b>	$1.34 \times 10^{-5}$	0.39	0.00061	7.75

\*Calculations are done by means of (1) computing Principal Components within each group of cases, i.e. individuals, muscle vector changes and constraints/segmentation in one individual; (2) computing variance within each analysis of the Principal Components; and (3) calculating percent of the variance in groups of cases for one individual in relation to the variance due to cases in different individuals.

### 3.4. The impact of muscle activation patterns on deformation

In the above analyses molar and incisor bites are each simulated using a different pattern of muscle activation (Table 2) and the resulting deformations clearly differ in strain contour maps and the PCAs of deformation. We assessed the extent to which the differences in deformation between bite points are due to differences in muscle activation pattern between molar and incisor bites by repeating the PCA among individuals loaded with identical muscle forces (those used for incisor bites in earlier studies, Table 1). Figure 4 presents a plot of the first two PCs from this test. Comparing it with Figure 3 where different muscle activation patterns were used for each bite, the scatters of individuals for the two bites overlap. Differences are much reduced, compared to the situation where different activation patterns are used to simulate each bite, indicating that a substantial proportion of the differences in deformation among bite points in Figure 3 (and in strain maps in Figure 2), is due to differences in muscle activation, rather than the effect of biting at different points.

**Figure 4.** PCA of residuals: data from 10 different individuals. Specimens loaded to simulate 1<sup>st</sup> incisor and 2<sup>nd</sup> molar biting using *the same* activation pattern (that used for I1: Table 2) for each bite. PC1/PC2 (71.4% of total variance). Individuals are shown by the same marker in each bite.



### 3.5. The association between form and deformation during simulated biting

The Mantel test of correlation between the matrix of Procrustes size and shape distances among unloaded crania of different individuals and matrices of Procrustes distances in size and shape among deformed models yields a high value,  $r=-0.73$  ( $P<0.001$ ) for incisor biting and a smaller value  $r=-0.28$  ( $P=0.006$ ) for molar biting. Thus mandibular deformation under simulated bites is significantly associated with mandibular form and this association appears to be even stronger for incisor bites.

Two block PLS analyses among the sizes and shapes of mandibles (Block 1) and their deformations for each of the two bites (Block 2) also indicate significant associations between form and deformation. Thus, for simulated incisor bites (Figure 5a, Table 12), the first axes explain 76% of the total covariance among blocks and the correlation between scores on these axes is,  $r=0.77$  ( $p$ -value = 0.006). The inset warpings of the mean form or deformation (Figure 5a) visualize the association between form and deformation: mandibles with taller bodies and square gonial angles deform with relatively greater lingual wishboning on the balancing side. Mandibles with a more obtuse gonial angle wishbone in the opposite (buccal) direction. Likewise the second axes, which explain 15% of the total covariance among blocks, show strong associations between form and deformation (Table 12), but are not shown here.

**Figure 5.** PLS of the unloaded mandibular sizes and shapes (Block 1) versus deformations in size and shape (Block 2) in the study of differences among individuals: (a) first axes of the PLS for the incisor bite; (b) first axes of the PLS for the second molar bite.

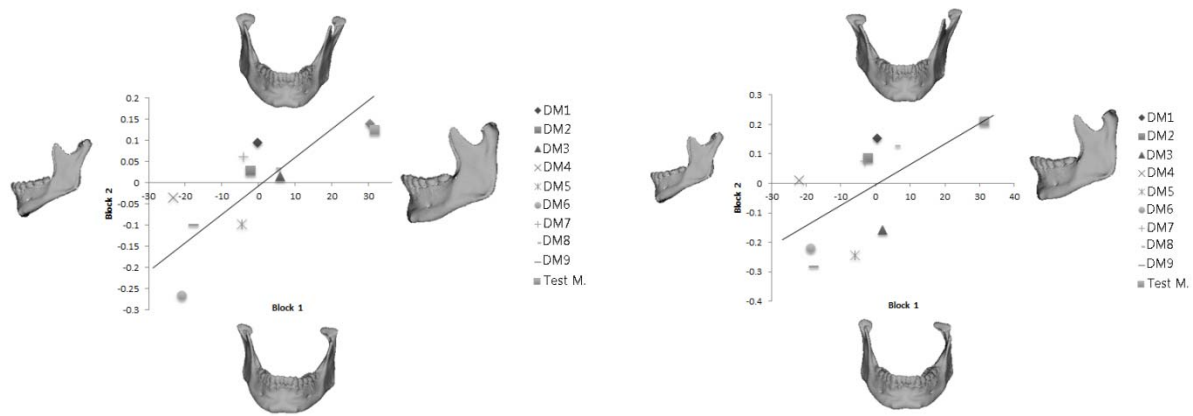


Table 12. Correlations among singular axes and the % of total variance in each block explained by the first two singular axes from 2-block PLS. Calculated as (size and shape variance on each axis/Total size and shape variance of each block) x100.

Tooth	Model	Axis 1		Axis 2	
		% of total variance	Correlation (p-value)	% of total variance	Correlation (p-value)
Incisor	Unloaded	42.4		51.5	
	Residuals of loaded	35.7	0.77 (0.006)	36.3	0.83 (0.002)
Second molar	Unloaded	39.9		14.0	
	Residuals of loaded	41.2	0.71 (0.014)	27.4	0.63 (0.037)

For simulated second molar bites (Figure 5b, Table 12), the first axes explain 75% of the total covariance among blocks and the correlation between scores on these axes is,  $r=0.71$  ( $p$ -value = 0.013). The inset warpings of the mean form or deformation (Figure 5b) indicate that mandibles with taller bodies and square gonial angles deform with relatively greater lingual wishboning on the balancing side and vice versa. Likewise the second axes which explain 13% of the total covariance among blocks, show strong associations between form and deformation (Table 10), but are not shown here.

Table 12 presents the proportion of the total variance in deformation due to biting and in mandibular form that is accounted for by the first and second singular axes in both PLS analyses. For incisor bites the first and second singular axes each account for ~36% of the total variance in deformation and 42-51% of the variance in form. In the molar biting simulations the first singular axes account for 41% of the total variance in deformation and 40% of the variance in form, while the second account for much less (14% and 27%). This indicates that more aspects of mandibular form variation are important in the resistance of incisor, than molar bites.

#### 4. Discussion

The aim of this paper has been to assess the sensitivity of FEA simulations of mandibular biting to varying modelling approaches and input variables. This is important because the form and functional performance of human mandible potentially provides a means by which mandibular loading history might be retrodicted and so, used to infer subsistence strategy and paramasticatory loading. This study uses FEA to assess functional performance and geometric morphometric approaches to the study of size and shape variations to compare form and deformation. FEA is an engineering technique that calculates stresses and strains produced in an object due to loads applied to it and so, potentially provides a means to predict and compare mandibular biomechanical performance. It is, however, subject to many sources of error that likely impact the resulting predictions of performance. Errors arise in adequately representing the gross anatomy and internal structure as well as in adequately representing variations in material properties throughout the bone, muscle loads and spatial constraints.

To assess how best to model and simulate biting and to understand what aspects of performance can reliably be predicted in comparative studies, which inevitably demand modelling approximations, we investigated the sensitivity of an FE model of a modern human mandible to simplifications in material properties and variations in boundary conditions and compared the findings with the variations in performance encountered among a sample of mandibles modelled in a standard way.

Our first hypothesis, H1: that variations in material properties and spatial constraints have no impact on performance assessed in terms of deformation and biting forces is falsified. Thus, from Table 7 it is clear that biting forces vary with variations in material properties and, in particular, with spatial constraints, as do the von Mises strain contour maps (Figure 2) and strain magnitudes at the 29 selected landmarks (Appendix, Figure A.1). Similarly, H2: that variations in muscle force vectors have no impact on performance assessed in terms of deformation and biting forces is also falsified (Table 8; Figure 2; Appendix, Figure A.2). Thus, how a mandible is modelled, loaded and constrained has an impact on the resulting FEA outputs. The relative contributions of these sources of error are assessed in Tables 10 and 11, which indicate that variations in muscle vectors, segmentation and constraints have a large impact on deformations as assessed by von Mises strains, and Procrustes size and shape distances among unloaded and loaded models.

These findings raise important considerations for comparative studies of mandibular form and function. However, if we wish to understand error in assessing comparative function, they need to be contextualised in relation to the range of variation in performance among a sample of mandibles. We approach this by first testing H3: that variations in mandibular form have no impact on performance assessed in terms of deformation and biting forces. Biting forces (Tables 7 and 8), von Mises Strains (Appendix, Figure A.3) and strain contour maps (Figure 2) all vary considerably, falsifying this hypothesis.

Mantel tests and 2-Block PLS analyses allow us to investigate how variations in mandibular form translate into variations in performance. The Mantel tests indicate that mandibular form and biting performance are significantly associated and this association appears to be stronger for incisor bites



than molar bites. The 2-block PLS analyses echo these findings in showing that form is strongly associated with deformation in both biting simulations. However while the first axes from these simulations explain similar proportions of the total variance in form and in deformation, the second axis from the incisor biting simulations explains a much greater proportion of variation in both form and deformation. These PLS analyses provide useful insights into what aspects of morphology are associated with resisting biting. These are useful in understanding how form relates to function (here biting resistance), and so has applications in many contexts beyond archaeology.

Having shown that modelling and loading decisions as well as mandibular form impact mandibular biting performance, it becomes important to assess the extent to which predicted differences in performance between subjects can reasonably be estimated, taking account of error in modelling and loading. To these ends we compare the variance in bite forces due to modelling and loading with the variance in bite forces among the small sample of mandibles. We find that the bite force varies due to differences in segmentation and constraints (Table 7), differences in muscle vectors (Table 8) and differences in form among individuals (Table 9). Muscle vector directions have a particularly large impact on the output force, especially when all are shifted together and with more vertical orientation of the vectors (when vectors shifted anteriorly) resulting in higher force output. The direction of the medial pterygoid muscle has the largest impact on the output of the incisor bite force.

Likewise when comparing von Mises strain contour maps (Figure 2) the variations due to modelling and loading decisions appear somewhat smaller than the differences among individuals. This is confirmed by the comparison of the variance in von Mises strains at 29 landmarks due to modelling and loading with that due to variation in our sample (Table 10). This shows that, on average, differences in modelling and loading result in 7.8% of the variance in strains among individuals.

These results are echoed and clarified by the PCA analysis of global modes and magnitudes of deformation which shows that the differences among different versions of the test mandible, segmented, loaded and constrained in different ways are small relative to the variations in deformation encountered among the sample of individuals. The variants of the test mandible occupy approximately 10-15% of the area in the plot occupied by different individuals (Figure 3). We further note (Figure 4) that muscle activation pattern has a marked effect on mode of deformation such that a large proportion of the difference in deformation that arises between simulated incisor and molar biting is the result of differences in muscle activation patterns, rather than bite point.

Our results therefore suggest that potential errors in segmentation and application of muscle force vectors, and constraints can have an appreciable effect on predictions of performance from FEA. In part they echo previous studies that have shown that allocation of material properties, and loadcase impact performance (Strait et al. 2005; Kober et al., 2004; Rayfield, 2007; Wroe et al., 2007; Wroe et al., 2010; Gröning et al. 2011a; Wood et al., 2011; Evans et al., 2012; Gröning et al. 2012; Parr et al., 2012; Toro-Ibacache et al., 2016; Godhino et al., 2017). However the errors are not large compared to the differences we expect to encounter in a sample.

If, in a single study, models are made from CT scans of similar resolution, segmentation is standardized, muscle load magnitudes and directions and constraints are held constant then we can anticipate reasonable results in terms of the *differences* in predicted performance among models. From previous validation studies (Toro-Ibacache et al. 2016, and Godihno et al. 2017), however, it is

evident that accurate prediction of strains from FEA is a far from trivial task and that most FEAs are unlikely to achieve this without detailed validation data against which to refine the model. Further accurate prediction of physiological strains presents the additional obstacles of accurately modelling the full complexity of physiological loadcases rather than simplified instantaneous loadings.

Although previous studies have found that while prediction of absolute strain magnitudes is very difficult (Toro-Ibacache et al. 2015, Godhino et al. 2017), FEA performs robustly in predicting relative strains over the surface of a model. Considering these findings and those from the present study a sensible approach for inter-individual comparative studies of mandibular biting performance is to build solid models, of one homogenous material (e.g. with the properties of cortical bone) in the knowledge they will reasonably predict relative strains but likely be too stiff (by unknown degree) to accurately predict strain magnitudes. If models are built similarly for all specimens in the sample and loaded and constrained identically, to ensure fair comparison, then FEA can be used for comparative studies of inter-individual variation in the mandibular form and function, where differences in performance, rather than actual performance are of interest. In effect, by fixing all variables other than mandibular form, studies can reasonably address the issue of how mandibular external form interacts with functional performance. This approach is directly applicable to within species variation while inter-species variation that involves large size differences and proportions of cancellous to cortical bone may need further investigation (Chamoli and Wroe, 2011). More sophisticated analyses await advances in methodology and more detailed knowledge of loading, internal architecture and variations in material properties.

## **5. Acknowledgements**

We would like to take this opportunity to extend our thanks to colleagues, who have provided us with material access and offered invaluable feedback on this study. These include Prof. A. Buzhilova from the Anuchin's Institute and Museum of Anthropology, Moscow State University, Russia. At CAHS we have been helped and supported by colleagues: Dr. Laura Fitton, Dr Sam Cobb and Dr Phil Cox.

This project could not have been conducted without the financial support of European Commission Research Grant No. PIIF-GA-2013-622846 (BIOMAN).

## **6. References**

- Beek, M., Koolstra, J.H., van Ruijven, L.J., van Eijden, T.M., 2000. Three-dimensional finite element analysis of the human temporomandibular joint disc. *J. Biomech.* 33, 307–316.
- Bourke, J., Wroe, S., Moreno, K., McHenry, C., Clausen, P. 2008. Effects of Gape and Tooth Position on Bite Force and Skull Stress in the Dingo (*Canis lupus dingo*) Using a 3-Dimensional Finite Element Approach. *PLOS One*, 5, e2200.
- Chamoli, U. and Wroe, S. 2011. Allometry in the distribution of material properties and geometry of the felid skull: why larger species may need to change and how they may achieve it. *J Theor Biol*, 283, 217–226.
- Chen, J., Akyuz, U., Xu, L., Pidaparti, R.M., 1998. Stress analysis of the human temporomandibular joint. *Med. Engin. & Phys.* 20, 565–572.

- Conti, M., Marconi, M., Campanile, G., Reali, A., Adami, D., Berchiolli, R., Auricchio, F. 2017. Patient-specific finite element analysis of popliteal stenting. *MECCANICA*, 52, 633-644. DOI: 10.1007/s11012-016-0452-9.
- Cox, P.G., Rayfield, E.J., Fagan, M.J., Herrel, A., Pataky, T.C., Jeffry, N. 2012. Functional Evolution of the Feeding System in Rodents. *PLOS One*, 4, e36299.
- Davis, J.L., Dumont, E.R., Strait, D.S., Grosse, I.R. 2011. An efficient method of modelling material properties using a thermal diffusion analogy: an example based on craniofacial bone. *PLOS One*, 6(2) e17004.
- Erdemira, A., Guess, TM., Halloran, J., Tadepalli, SC., Morrison, TM. 2012. Considerations for reporting finite element analysis studies in biomechanics. *J. Biomech.*, 45, 625-633, DOI: 10.1016/j.jbiomech.2011.11.038
- Evans, S.P., Parr, W.C.H., Clausen, P.D., Jones, A., Wroe, S., 2012. Finite element analysis of a micromechanical model of bone and a new 3D approach to validation. *J. Biomech.* 45, 2702–2705.
- Fitton, L. C., PrôA, M., Rowland, C., Toro-ibacache, V., & O'Higgins, P. 2015. The impact of simplifications on the performance of a finite element model of a *Macaca fascicularis* cranium. *Anat. Rec.*, 298, 107-121
- Godinho, R.M., Toro-Ibacache, V., Fitton, L.C., O'Higgins, P. 2017. Finite element analysis of the cranium: validity, sensitivity and future directions. *Compt. Rend. Palevol.*, 16 , 600-612, DOI:10.1016/j.crpv.2016.11.002
- Gröning, F., Liu, J., Fagan, M. J., & O'Higgins, P. 2011a. Why do humans have chins? Testing the mechanical significance of modern human symphyseal morphology with finite element analysis. *Am. J. Phys. Anth.*, 144, 593-606.
- Gröning, F., Fagan, M. J., & O'Higgins, P. 2011b. The effects of the periodontal ligament on mandibular stiffness: a study combining finite element analysis and geometric morphometrics. *J. Biomech.*, 44, 1304-1312.
- Gröning, F., Fagan, M., & O'Higgins, P. 2012. Modeling the human mandible under masticatory loads: which input variables are important? *Anat. Rec.*, 295, 853-863.
- Koolstra, J.H., van Eijden, T.M.G.J., 1997. Dynamics of the human masticatory muscles during a jaw open–close movement. *J. Biomech.* 30, 883–889.
- Kober, C., Erdmann, B., Hellmich, C., Sader, R., Zeilhofer, H.-F. 2004. Anisotropic Simulation of the Human Mandible. *ZIB-Report* 4, 1-13.
- Koolstra, J.H., van Eijden, T.M., 2005. Combined finite-element and rigid-body analysis of human jaw joint dynamics. *J. Biomech.* 38, 2431–2439.
- Ledogar, J.A., Dechow, P.C., Wang, Q., Gharpure, P.H., Gordon, A.D., Baab, K.L., Smith, A.L., Weber, G.W., Grose, I.R., Ross, C.F., Richmond, B.G., Wright, B.W., Byron, C., Wroe, S., Strait, D. 2016.

Human feeding biomechanics: performance, variation, and functional constraints. PeerJ, DOI: 10.7717/peerj.2242.

Ledogar, J.A., Benazzi, S., Smith, A.L., Weber, G.W., Carlson, K.B., Dechow, P.C., Grosse, I.R., Ross, C.F., Richmond, B.G., Wright, B.W., Wang, Q., Byron, C., Carlson, K.J., de Ruiter, D.J., Pryor, L.C., Strait, D.S. 2017. The biomechanics of bony facial “buttresses” in South African australopiths: an experimental study using finite element analysis. *Anat. Rec.*, 300, 171-195.

Marcé-Nogué, J., Püschel, T. A., & Kaiser, T. M. 2017. A biomechanical approach to understand the ecomorphological relationship between primate mandibles and diet. *Sci. Rep.*, 7, 8364, DOI: 10.1038/s41598-017-08161-0.

Milne, N., O’Higgins, P. 2012. Scaling of form and function in the xenarthran femur: a 100-fold increase in body mass is mitigated by repositioning of the third trochanter. *Proc. R. Soc. B* DOI:10.1098/rspb.2012.0593.

Moreno, K., Wroe, S., Clausen, P., McHenry, C., D’Amore, D.C., Rayfield, E.J., Cunningham, E. (2008) Cranial performance in the Komodo dragon (*Varanus komodoensis*) as revealed by high-resolution 3-D finite element analysis. *J. Anat.* 212, 736–746.

Nelson, G.J., 1986. Three dimensional computer modelling of the human mandibular biomechanics. M.Sc. Thesis, University of British Columbia, Vancouver, Canada.

O’Connor C.F., Franciscus R.G., Holton N.E. 2005. Bite force production capability and efficiency in Neandertals and modern humans. *Am. J. Phys. Anthr.* 127, 129–151, DOI 10.1002/ajpa.20025.

O’Higgins, P., Milne, N. 2013. Applying geometric morphometrics to compare changes in size and shape arising from finite elements analyses. *Hystrix*, DOI:10.4404/hystrix-24.1-6284.

O’Higgins, P., Cobb, S.N., Fitton, L.C., Gröning, F., Philips, R., Liu, J., Fagan, M.J. 2011. Combining geometric morphometrics and functional simulation: An emerging toolkit for virtual functional analyses. *J. Anat.* 218, 3–15.

O’Higgins, P., Fitton, L.C., Phillips, R., Shi, J.F., Liu, J., Gröning, F., Cobb, S.N., Fagan, M.J. 2012. Virtual functional morphology: Novel approaches to the study of craniofacial form and function. *Evol Biol.* DOI 10.1007/s11692-012-9173-8.

Parr, W.C.H., Wroe, S., Chamoli, U., Richards, H.S., McCurry, M.R., Clausen, P.D., McHenry, C., 2012. Toward integration of geometric morphometrics and computational biomechanics: new methods for 3D virtual reconstruction and quantitative analysis of finite element models. *J. Theor. Biol.* 301, 1–14.

Peterson, J., Dechow, P.C. 2003. Material properties of the human cranial vault and zygoma. *Anat. Rec. Part A* 274A, 785-797.

Rayfield, E.J., 2007. Finite element analysis and understanding the biomechanics and evolution of living and fossil organisms. *Ann. Rev. EarthPlanet. Sci.* 35, 541–576.

Richmond, B.G., Wright, B.W., Grosse, L., Dechow, P.C., Ross, C.F., Spencer, M.A., Strait, D.S., 2005. Finite element analysis in functional morphology. *Anat. Rec. Part A* 283A, 259–274.

Smith, A.L., Benazzi, S., Ledogar, J.A., Tamvada, K., Pryor Smith, L.C., Weber, G.W., Spencer, M.A., Dechow, P.C., Grosse, I.R., Ross, C.F., Richmond, B.G., Wright, B.W., Wang, Q., Byron, C., Slice, D.E., Strait, D.S. 2015a. Biomechanical implications of intraspecific shape variation in chimpanzee crania: moving towards an integration of geometric morphometrics and finite element analysis. *Anat. Rec.* 298, 122-144.

Smith, A.L., Benazzi, S., Ledogar, J.A., Tamvada, K., Pryor Smith, L.C., Weber, G.W., Spencer, M.A., Lucas, P.W., Michael, S., Shekeban, A., Al-Fadhalah, K., Almusallam, A.S., Dechow, P.C., Grosse, I.R., Ross, C.F., Madden, R.H., Richmond, B.G., Wright, B.W., Wang, Q., Byron, C., Slice, D.E., Wood, S., Dzialo, C., Berthaume, M.A., van Castern, A., Strait, D.S. 2015b. The feeding biomechanics and dietary ecology of *Paranthropus boisei*. *Anat. Rec.* 298, 145-167.

Spencer, M.A., Demes, B. 1993. Biomechanical analysis of masticatory system configuration in Neandertals and Inuits. *Am. J. Phys. Anth.*, 91, 1–20, DOI:10.1002/(ISSN)1096-8644.

Strait, D.S., Weber, G.W., Neubauer, S., Chalk, J., Richmond, B.G., Lucas, P.W., Spencer, M.A., Schrein, C., Dechow, P.C., Ross, C.F., Grosse, I.R., Wright, B.W., Constantino, P., Wood, B.A., Lawn, B., Hylander, W.L., Wang, Q., Byron, C., Slice, D.E., Smith, A.L., 2009. The feeding biomechanics and dietary ecology of *Australopithecus africanus*. *Proc. Natl. Acad. Sci. U.S.A.* 106, 2124–2129.

Strait, D. S., Wang, Q., Dechow, P.C., Ross, C.F., Richmond, B.G., Spencer, M.A., Patel, B.A. 2005. Modeling elastic properties in finite-element analysis: How much precision is needed to produce an accurate model? *Anat. Rec.*, 283, 275-287.

Strait, D.S., Constantino, P., Lucas, P.W., Richmond, B.G., Spencer, M.A., Dechow, P., Ross, C.F., Grosse, I.R., Wright, B.W., Wood, B.A., Weber, G.W., Wang, Q., Byron, C., Slice, D.E., Chalk, J., Smith, A.L., Smith, L.C., Wood, S., Berthaume, M., Benazzi, S., Dzialo, C., Tamvada, K., Ledogar, J. 2013. Viewpoints: diet and dietary adaptations in early hominins: the hard food perspective. *Am. J. Phys. Anth.* 151, 339-355.

Tanne, K., Tanaka, E., Sakuda, M., 1991. The elastic modulus of the temporomandibular joint disc from adult dogs. *J. Dent. Res.* 70, 1545–1548.

Toro-Ibacache, V., Fitton, L.C., Fagan, M.J., O'Higgins, P., 2015. Validity and sensitivity of a human cranial finite element model: implications for comparative studies of biting performance. *J. Anat.* DOI: 10.1111/joa.12384.

Toro-Ibacache, V., Fitton, L.C., Fagan, M.J., O'Higgins, P., 2016. Validity and sensitivity of a human cranial finite element model: implications for comparative studies of biting performance. *J. Anat.* 228, 70-84.

Tsouknidas, A., Jimenez-Royo, L., Karatsis, E., Michailidis, N., Mitsiadis T.A. 2017. A bio-realistic finite element model to evaluate the effect of masticatory loadings on mouse mandible-related tissues. *Front. Physiol.* 8, Article 273, DOI: 10.3389/fphys.2017.00273

- van Eijden TM, Koolstra JH, Brugman P. 1995. Architecture of the human pterygoid muscles. *J Dent Res*, 74, 1489–1495.
- van Eijden TM, Koolstra JH, Brugman P. 1996. Three-dimensional structure of the human temporalis muscle. *Anat Rec*, 246, 565–572.
- Von Cramon-Taubadel, N. 2011. Global human mandibular variation reflects differences in agricultural and hunter-gatherer subsistence strategies. *PNAS*, 108, 19546-19551.
- Wood, S.A., Strait, D.S., Dumont, E.R., Ross, C.F., Grosse, I.R., 2011. The effects of modeling simplifications on craniofacial finite element models: the alveoli (tooth sockets) and periodontal ligaments. *J. Biomech.* 44, 1831–1838.
- Wroe, S., Moreno, K., Clausen, P., Mchenry, C., Curnoe, D., 2007. High-resolution three-dimensional computer simulation of hominid cranial mechanics. *Anat. Rec.* 290, 1248–1255.
- Wroe, S., Ferrara, T. L., McHenry, C. R., Curnoe, D., & Chamoli, U. 2010. The craniomandibular mechanics of being human. *Proc. R. Soc. Lon. B-Biol.Sci.* 277, 3579–3586, rspb20100509.
- Zink, K.D., Lieberman, D.E. 2016. Impact of meat and Lower Paleolithic food processing techniques on chewing in humans. *Nature*, 531, 500–503 DOI: 10.1038/nature16990.